Effects of the different Supported Structures on Tubular Solid Oxide Fuel Cell Performance

Zidong Yu[1,2,*], Shengji Liu[1,*], Fa Zheng[3], Yuhong Ding[3]

[1] School of Automobile and Traffic Engineering, Jiangsu University, Zhenjiang, Jiangsu 212013, China;
[2] School of Energy and Power Engineering, Jiangsu University of Science and Technology, Zhenjiang, Jiangsu 212003, China.
[*]E-mail: yuzidong@just.edu.cn
[3] Jiangsu Zhongjing New Energy Science & Technology Research Center, Zhenjiang, Jiangsu 212013, China.

A comprehensive two-dimensional model has been developed to investigate the performance of tubular solid oxide fuel cell (T-SOFC) stack with different supported structures. The discrepancy between the anode-supported tubular SOFC (AST-SOFC) stack and the cathode-supported tubular SOFC (CST-SOFC) stack are examined by varying temperature, electrical conductivity, porosity, contact resistance and output voltage. The results illustrate that the different supported structures have an significant influence on the performance of stack. The performance of CST-SOFC stack is much better than AST-SOFC stack for any aforementioned working parameters. Especially in lower temperature, smaller cathode conductivity, larger cathode porosity and lower output voltage, the advantage is more outstanding.

1. INTRODUCTION

In recent years, in order to deal with the crisis of energy resource and environmental pollution, countries around the world are actively developing clean, efficient and environmentally friendly new energy technology, such as solar energy, nuclear power and wind energy. Solid Oxide Fuel Cell (SOFC) exhibits a great advantages and potential in solution of energy crisis and environmental

pollution due to its high efficiency of energy conversion, lower or zero emissions of pollutants, flexibility in fuel choice and without noble metal catalytic, etc[1-4]. Therefore, it has made great strides in worldwide, which is considered to be the most developed renewable source in the 21st century [5, 6].

There are many choices in its structure and shape design due to all-solid-state structure of SOFC. Therefore, it can be designed according to different usage requirements and environments. Moreover, the design of SOFC should be persisted in reliable performance, easy to enlarge and maintenance as well as reasonable price principle. At present, the major SOFC types include the planar SOFC and the tubular SOFC [7]. The Planar SOFC is of the simple structure, preparation process, short current paths and high energy conversion efficient [8]. However, planar SOFC sealing at high temperature is difficult, which leads to poor thermal cycling performance. And thus, it is a huge challenge for the reliability and long-term stability of SOFC. In contrast, tubular SOFC (T-SOFC)shows the advantages of simple sealing, high volume energy density, better thermal shock resistance and mechanical strength, easy in series or parallel mode of each single cell assembled into large scale fuel cell system[7-9].Furthermore, long-term stability tests with T-SOFC up to 69,000 h were reported[10], so the research on its structure and performance has been the frontier and hot direction in the research of fuel cell.

In published literatures, there are some studies about the CST-SOFC and AST-SOFC. Li et al. [11] established a CST-SOFC model and investigate the influence of temperature and species concentration on the electrochemical properties of CST-SOFC. Lee et al. [12] designed a new cell structure to reduce the high ohmic loss and increase the uniform gas distribution in anode-supported micro-tubular SOFC. Cui et al. [13] compared the different current collector types and found the current collector type played a key role in improving the cell performance. Zhou et al.[14] developed an AST-SOFC model and pointed out that the maximum output power density of the cell at 800℃increased from 266.7 to 306 mW/cm^2 with the fuel gas pressure rising from 1 atm to 6 atm. Jia et al. [15] proposed an electrochemical model of the T-SOFC stack with radiation heat transfer inside tube, and showed that reducing the electrolyte thickness and increasing the mean pore radius of the electrode are beneficial to increasing the cell performance.

Su et al. [16] compared the performance difference of the anode-supported planar SOFC (ASP-SOFC) stack with that of the cathode-supported planar SOFC (CSP-SOFC) stack from gas concentration distribution, potential distribution to temperature distribution. At the same time, the discrepancy between ASP-SOFC and CSP-SOFC are further verified by changing contact resistance rib size, and pitch width. The results indicated that the output of the CSP-SOFC with the optimal rib size was obviously higher than the that of ASP-SOFC for different pitch widths and contact resistances. But, whether this conclusion is applicable to the T-SOFC, there is currently no found in the existing literature. Therefore, the feasibility of the research in this area has not been confirmed yet and this is also the purpose and essence of this paper.

In order to further verify the performance merits between AST-SOFC and CST-SOFC, a 2D model of SOFC is established firstly. The performance analyses and comparing of the fuel cells mentioned above are carried out based on specified geometries of the T-SOFC, and then illustrates the influence of the cell design on the cell performance.

2. MODEL

2.1 Geometry Model
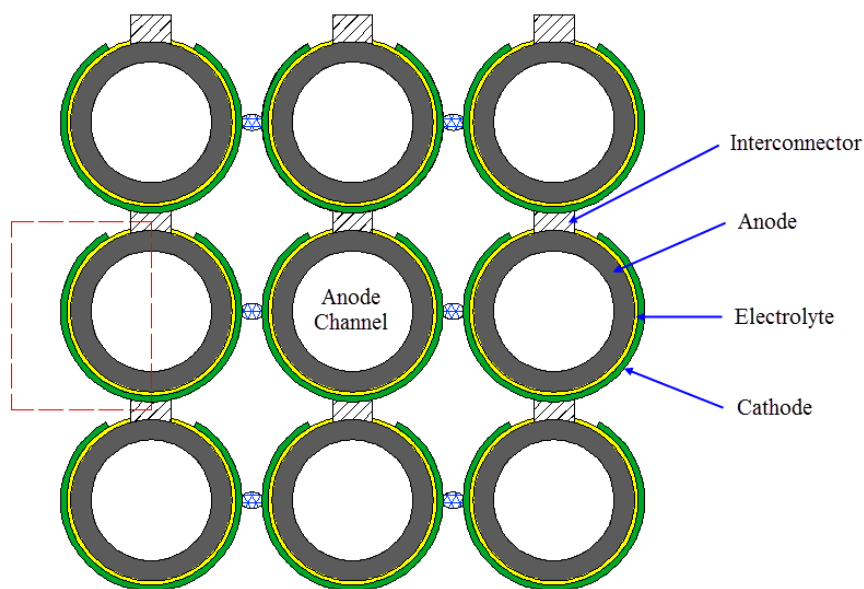
Figure 1. The cross-section of the T-SOFC
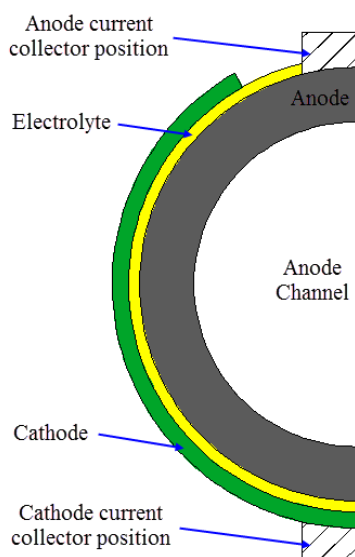
Figure 2. Mode structure

Generally, the T-SOFC stack includes many single cells and interconnectors. An single cell has a electrolyte, anode and cathode, as shown in Fig. 1. According to the symmetry of tubular SOFC structure, this work selects half of the repeating unit as computational domain, as shown in Fig. 2. The geometric parameters involved in the simulation process are listed in Table 1.

Table 1. Geometric parameters

Cell component	Value (μm)
anode-supported	
anode thickness	1000
electrolyte thickness	20
cathode thickness	50
cathode-supported	
anode thickness	50
electrolyte thickness	20
cathode thickness	1000
inside diameter	9000
interconnect width	3000
interconnect height	2500

2.2 Governing equations

2.2.1 Governing equations of Gas transport in electrodes

The molar flux of species in electrodes may be expressed as [17,18]：

$$N_i = -\frac{D_{12}^{\text{eff}} D_{iK}^{eff}}{D_{12}^{\text{eff}} + x_1 D_{2K}^{eff} + x_2 D_{1K}^{eff}} \nabla c_i$$

$$-c_i \left(\frac{D_{1K}^{eff} D_{2K}^{eff}}{RT c_{tot} \left(D_{12}^{\text{eff}} + x_1 D_{2K}^{eff} + x_2 D_{1K}^{eff} \right)} + \frac{k}{\mu} \right) \nabla p \qquad （1）$$

$$= -D_i \nabla c_i - c_i \frac{k^{'} \nabla p}{\mu} = N_i^{diffusion} + N_i^{convection}$$

Because the all parameters symbols in this paper are same to that in reference[17], the meaning of parameters symbols don't given here again.

D_{ij}^{eff} and D_{ik}^{eff} can be expressed as follows [17,19]:

$$D_{ij}^{eff} = \frac{\varepsilon}{\tau} \frac{3.198 \times 10^{-8} T^{1.75}}{p \left(v_i^{1/3} + v_j^{1/3} \right)^2} \left(\frac{1}{M_i} + \frac{1}{M_j} \right)^{0.5} \quad （2）$$

$$D_{ik}^{eff} = \frac{\varepsilon}{\tau} \frac{2}{3} r_g \sqrt{\frac{8RT}{\pi M_i}} \quad （3）$$

2.2.2 Governing equations of charge conductive

Electron current density and ion current density can be expressed as [17]:

$$\nabla \cdot i_{el} = \nabla \cdot \left(-\sigma_{el}^{eff} \nabla \phi_{el} \right) = S_{current} \quad （4）$$

$$\nabla \cdot i_{io} = \nabla \cdot \left(-\sigma_{io}^{eff} \nabla \phi_{io} \right) = -S_{current} \quad （5）$$

2.2.3 Butler-Volmer equations

For Ni/YSZTPB the charge transfer current density(i_{trans}) can be written as [17,20]:

$$i_{trans}^{an} = i_{ref}^{an} \exp\left(-\frac{E_{H_2}}{R}\left(\frac{1}{T} - \frac{1}{T_{ref}}\right)\right)\left(\frac{p_{H_2}^{TPB} p_{H_2O}^{TPB}}{p_{H_2}^0 p_{H_2O}^0}\right)\left[\exp\left(\frac{2\alpha_f^{an} F}{RT}\eta_{act}^{an}\right) - \exp\left(-\frac{2\beta_r^{an} F}{RT}\eta_{act}^{an}\right)\right] \quad (6)$$

For LSM/YSZTPB, i_{trans} can be written as [17,20]:

$$i_{trans}^{ca} = i_{ref}^{ca} \exp\left(-\frac{E_{O_2}}{R}\left(\frac{1}{T} - \frac{1}{T_{ref}}\right)\right)\left(\frac{p_{O_2}^{TPB}}{p_{O_2}^0}\right)^{0.25}\left[\exp\left(\frac{2\alpha_f^{ca} F}{RT}\eta_{act}^{ca}\right) - \exp\left(-\frac{2\beta_r^{ca} F}{RT}\eta_{act}^{ca}\right)\right] \quad (7)$$

The values of input parameters used in the model are shown in Table 2.

Table 2. Model input parameters

Descriptions	Symbol	Value
Temperature (℃)	T	1000
Operation voltage (V)	V_{op}	0.7
Tortuosity factor	τ	3.5
Porosity	ε	0.3
Mole fraction of fuel	x_{H_2}, x_{H_2O}	0.7, 0.3
Mole fraction of air	x_{O_2}, x_{N_2}	0.21, 0.79
Inlet concentration of fuel (mol m^{-3})	$c_{H_2}^0, c_{H_2O}^0$	6.7, 2.87
Inlet concentration of air (mol m^{-3})	$c_{O_2}^0, c_{N_2}^0$	2.01, 7.56
Activation energies for the anode (J mol^{-1})	E_{H_2}	1.2 e^5
Activation energies for the cathode (J mol^{-1})	E_{O_2}	1.3 e^5
Exchange transfer current density of anode(A m^{-1})	i_{ref}^{an}	2000
Exchange transfer current density of cathode (A m^{-1})	i_{ref}^{ca}	860
Reaction symmetric factor for anode	$\alpha_f^{an}, \beta_r^{an}$	2, 1
Reaction symmetric factor for cathode	$\alpha_f^{ca}, \beta_r^{ca}$	1.5, 1

2.3 Boundary conditions

Different boundary conditions have to be set to solve the coupled partial differential equations mentioned above, as described in Table 3.

Table 3. Boundary settings in numerical simulation

Location	Boundary conditions (mass ,charge)	Boundary type
Anode / channel	$c^0 = p_{H_2}^0 / R / T$	H_2 molar concentration
	$c^0 = p_{H_2O}^0 / R / T$	H_2O molar concentration
Anode / rib	$E_0 \left(= 1.1\text{V} \right)$	Reference potential
	0.01 Ω cm^2- 0.05 Ω cm^2	Contact resistance
Anode / electrolyte	$-i_{trans}^{an} \lambda_{TPB}^A / 2F$	H_2 Inward molar flux
	$i_{trans}^{an} \lambda_{TPB}^A / 2F$	H_2O Inward molar flux
	$-i_{trans}^{an} \lambda_{TPB}^A$	Inward current flow(Electronic transfer)
	$i_{trans}^{an} \lambda_{TPB}^A$	Interior current source(Ionic transfer)
Cathode / channel	$c^0 = p_{O_2}^0 / R / T$	O_2 molar concentration
	$c^0 = p_{N_2}^0 / R / T$	N_2 molar concentration
Cathode / rib	V_{OP}	Reference potential
	0.01 Ω cm^2- 0.05 Ω cm^2	Contact resistance
Cathode / electrolyte	$-i_{trans}^{ca} \lambda_{TPB}^A / 4F$	O_2 Inward molar flux
	0	N_2 Inward molar flux
	$i_{trans}^{ca} \lambda_{TPB}^A$	Inward current flow(Electronic transfer)
	$-i_{trans}^{ca} \lambda_{TPB}^A$	Interior current source(Ionic transfer)
All others	-	Insulation / Electric insulation

Note: λ_{TPB}^A is the area-specific TPB length, insulation means no flow through the border and electric insulation means that the normal component of the electric current is zero [17].

3. RESULTS AND DISCUSSION

In order to research the difference between the AST-SOFC and CST-SOFC, two 2D models were developed with the same basic model parameters listed in Table 1 except the thickness of electrodes. The anode and cathode thickness of AST-SOFC stack are 1000 and 50 μm，respectively, which for CST-SOFC stack are 50 and 1000 μm, respectively. Based on the established physical model, two different electrode supported structures are compared in terms of operating temperature, electrical conductivity, porosity, contact resistance and output voltage.

3.1 Effect of Operating Temperature

Temperature plays a key role in affecting the performance of the cell, while the high temperature is conducive to the improvement of cell performance, as illustrated in Fig. 3. The output current density increases 15.7% and 3.2% from T=850℃ to T=1150℃ for the AST-SOFC stack and CST-SOFC stack, respectively. This results are similar with the experimental data reported in references[21-23]. Ullah et al. reported that the output power density were increased about 18.80% when operating temperature increased from 650 °C to 750 °C. López-Robledo et al. fabricated micro-tubular SOFC and founded that the peak power densities of cell was 335 mW cm^{-2} at 750 °C and 525 mW cm^{-2} at 800 °C. It is shown that the performance of AST-SOFC is influenced remarkably by temperature. It is attributed to the fact that the electrode conductivity increases with the increase of the temperature, while thinner cathode of AST-SOFC is more susceptible to temperature. It appears that the performance of CST-SOFC has been better than the performance of AST-SOFC at different operating temperatures, especially under low operating temperature, the advantage is more obvious.
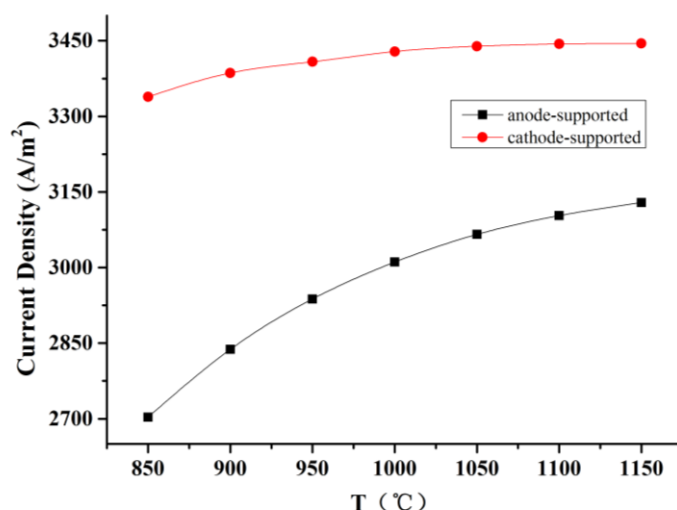
Figure 3. AST-SOFC stack and the CST-SOFC stack performance comparison with different operating temperature.

3.2 Effect of Electrical Conductivity

Fig. 4 shows the effect of electrical conductivity on the AST-SOFC performance and CST-SOFC. The output current density of AST-SOFC and CST-SOFC increases with the increase of anode electrical conductivity, but the current density of AST-SOFC is slightly affected by electrical conductivity. This results are similar with the data reported in references[17], which founded that the output of AST-SOFC wasn't almost change when anode conductivity increased from 4510 S m^{-1} to 45100 S m^{-1}. For AST-SOFC, the anode is thick. Moreover, the anode conductivity is quite large. As a result, the effect of anode conductivity on AST-SOFC performance is almost negligible when anode conductivity is lager.
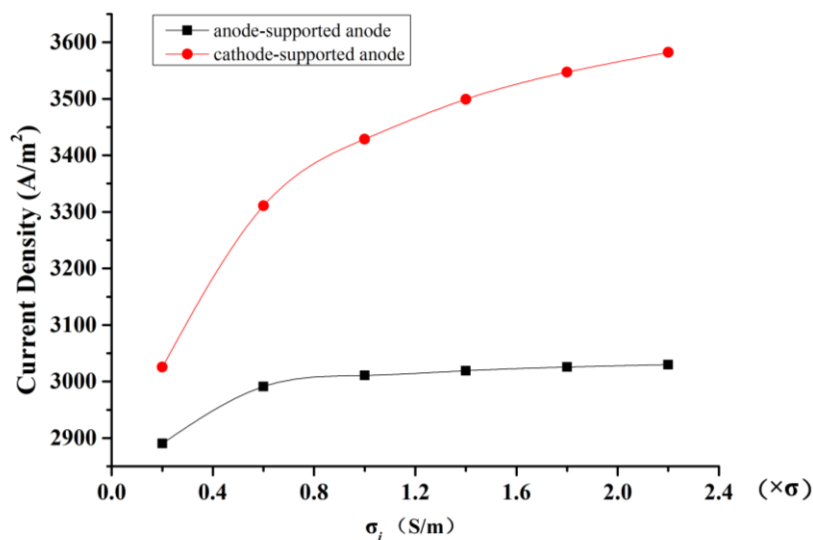
(a) anode
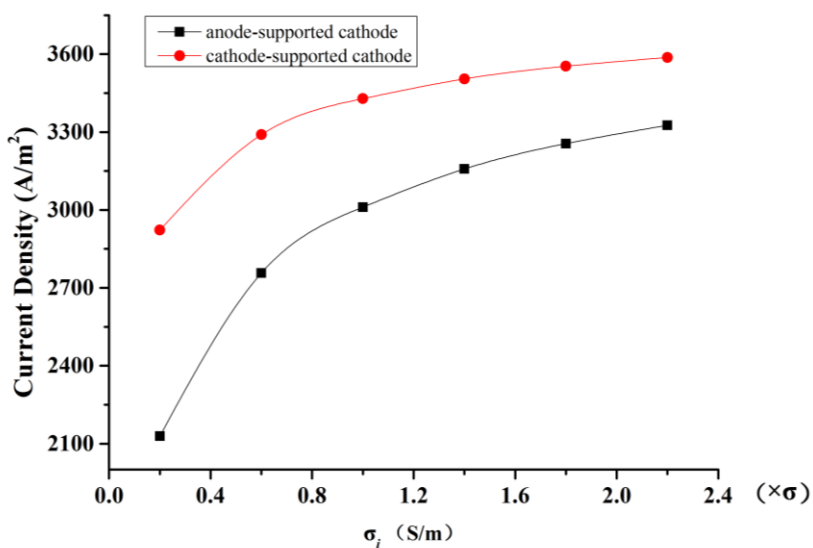
(b) cathode

Figure 4. AST-SOFC stack and the CST-SOFC stack performance comparison with different electrical conductivity.

The different effects of the anode conductivity on the AST-SOFC and CST-SOFC performance are due to the anode thickness difference. Furthermore, the current density of CST-SOFC is greatly improved compared with AST-SOFC, as can be seen in Fig. 4(a). When the anode electrical conductivity is 2.2σ S/m, the output current density of the CST-SOFC increases 18.2% compared with AST-SOFC. While the anode electrical conductivity is 0.2σ S/m, it increases only 4.7%. Clearly, the bigger the anode electrical conductivity is, the more outstanding the performance advantages of the CST-SOFC is.

Fig. 4(b) describes the relationship between output current density and cathode conductivity. It is obvious that the change of cathode conductivity has a profound influence on the output performance of cell. With the cathode conductivity varying from 0.2σ S/m to 2.2σ S/m, the output current density of CST-SOFC is superior to the AST-SOFC. Furthemore, the performance advantage of CST-SOFC is more significant in the smaller cathode conductivity situation.

3.3 Effect of Porosity

Porosity is an important parameter in describing difficulty lever of gas transmission in the electrode. Fig.5 describes the correspondence relationship between the porosity and the current density of different cell designs. As shown in Fig. 5(a), the output current density of AST-SOFC first ascended and the descended with the increment of anode porosity, but is slightly affected by anode porosity. However, the output current density of CST-SOFC is decreased gradually at a more conspicuous rate with increasing anode porosity. For the change of anode porosity, the reason for the opposite trend of the current density is that the anode in anode supported SOFC is thicker, the diffusion of fuel gas caused a greater concentration polarization.
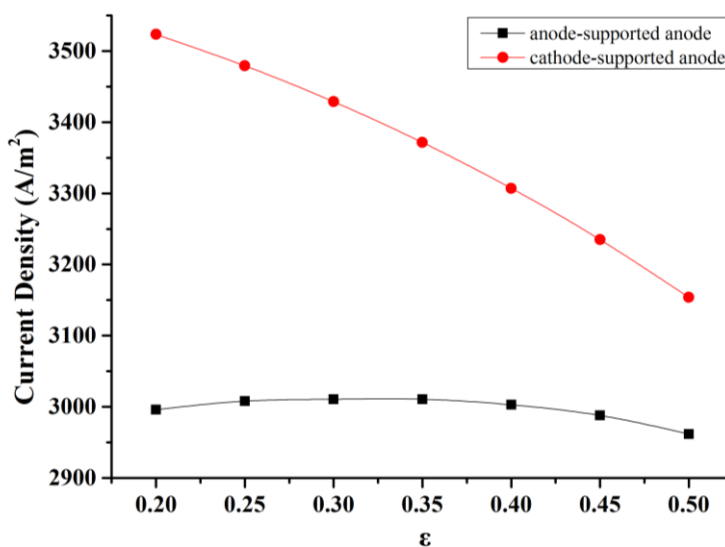
(a) anode
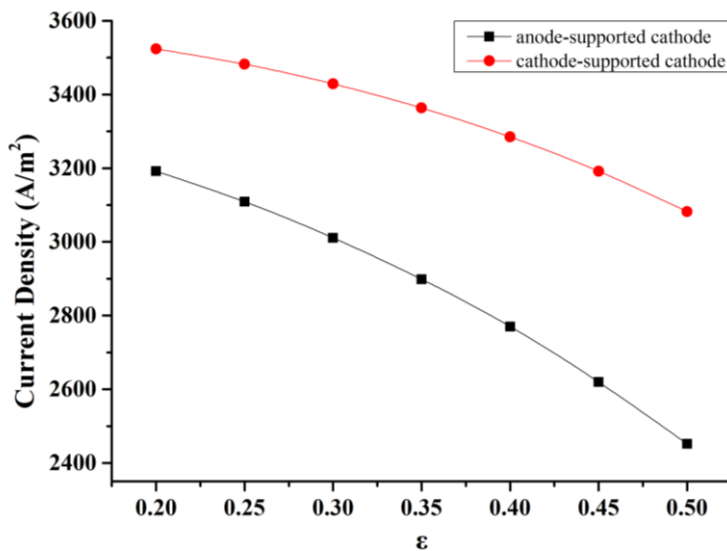
(b) cathode

Figure 5. AST-SOFC stack and the CST-SOFC stack performance comparison with different porosity.

And thus, increasing the porosity is favorable to the diffusion of gas, which can reduce the concentration polarization and raise the output current density. However, it is a quite different situation for the thinner anode of CST-SOFC. The increase of porosity will lead to a serious decline in electrical conductivity, which makes the ohmic polarization significantly increased. So, there exists the phenomenon of current density rapid reduction with the porosity increase. The results are similar with the findings in the reference [24]. The effective conductivities is the function of porosity with Bruggeman factor of $\gamma=3.5$, which means that conductivity reduce sharply with the decrease of porosity.

In Fig. 5(b), the cell output of AST-SOFC and CST-SOFC decrease by the increase of cathode porosity. The reason is that the cathode conductivity is lower, and thus the increase of porosity will cause of seriously reduced cathode conductivity. Further analysis of Fig.5 (a) and (b) show that the output current density of CST-SOFC is maintaining at a higher level comparing with AST-SOFC, especially when the anode porosity equals 0.2 and the cathode porosity equals 0.5. The corresponding current density growth percentage is 17.6% and 25.7% respectively.

3.4 Effect of Contact Resistance

Fig. 6 shows the effect of contact resistance on output current density. As expected, the output current density reduces with the increase of the contact resistance. When the contact resistance varies from 0.01 Ω cm^2 to 0.05 Ω cm^2, the output current density decrease by 59.5%, 62.8%, 59.6% and 62.8% for the anode/cathode of AST-SOFC and CST-SOFC, respectively. The results are similar with the findings in the reference [25]. The current densities decreases from 6909 to 5611 A m^{-2} with the increase of contact resistance from 0.01 to 0.05 Ω cm^2. Therefore, it is advisable to decrease the

contact resistance between the interconnector and electrode so as to improve the cell output. When the contact resistance is 0.01Ω cm^2, comparing with AST-SOFC, the output current density of CST-SOFC rose by 13.9% at the anode sideand 14.0 % at the cathode side. Obviously, CST-SOFC provides considerably better performance than AST-SOFC.
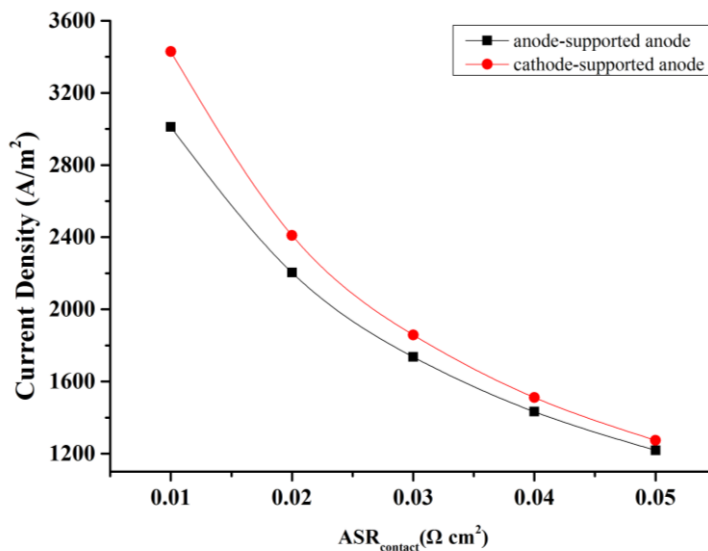
(a) anode
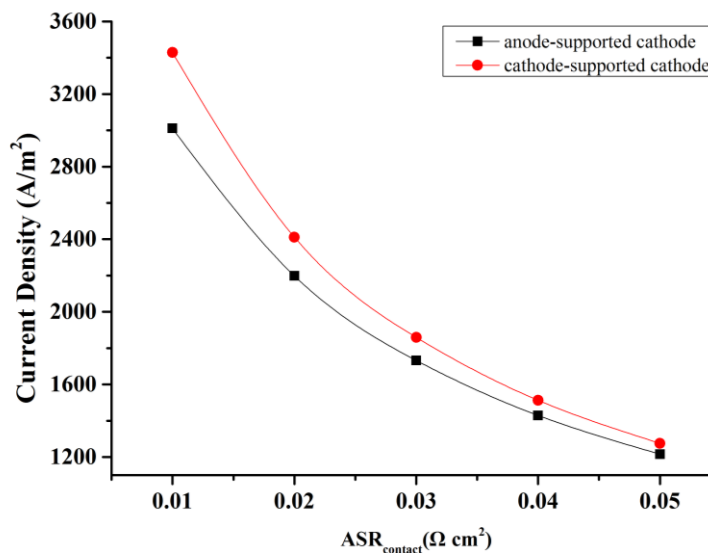
(b) cathode

Figure 6. AST-SOFC stack and the CST-SOFC stack performance comparison with different contact resistance.

3.5 Effect of Output Voltage (Vop)
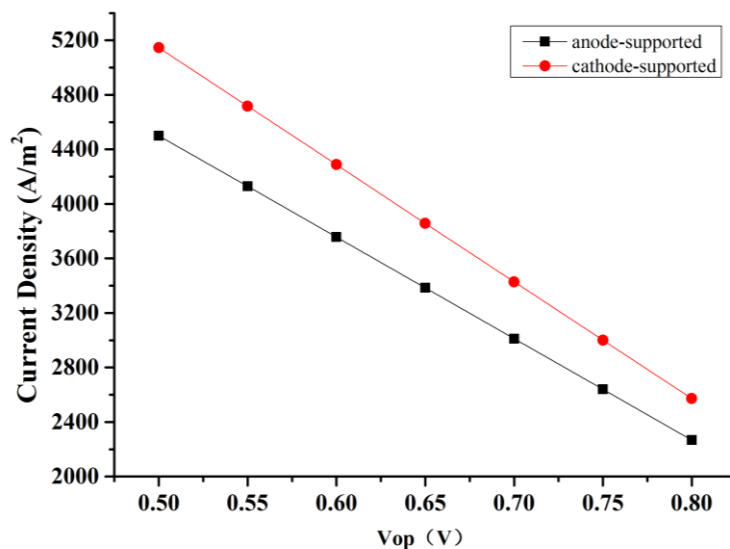
Figure 7. AST-SOFC stack and the CST-SOFC stack performance comparison with different Vop.

To analyze the influence of Vop on T-SOFC, different Vop values are selected so that the Vop changes from 0.5 V to 0.8 V. As is depicted in the Fig.7, the output current density of AST-SOFC and CST-SOFC decreases rapidly with increasing of Vop. Clearly, the cell output is strongly dependent on the Vop. This results is similar with the findings in reference [26].

A further observation indicates that the current density curve of CST-SOFC is in the above for different output voltage. Accordingly, it is important to know that the change of supported structure of the cell can effectively promote the improvement of the performance of the SOFC stack. What's more, this superiority is more apparent when Vop is 0.5 V. Compared with AST-SOFC, the output current density of CST-SOFC increase by 14.4%.

4. CONCLUSIONS

In this study, the 2D mathematical model of gas transport and charge transport for T-SOFC has been established to investigate the differences between the AST-SOFC and CST-SOFC. The performance difference between AST-SOFC stack and CST-SOFC are compared from the temperature, electrical conductivity, porosity, contact resistance and output voltage respectively. The results indicate that the performance of SOFC stack can be significantly improved by appropriately increasing the operating temperature and electrode conductivity, at the same time reducing the porosity of porous electrode, contact resistance and the output voltage. Moreover, the performance of CST-SOFC stack is much better than AST-SOFC stack for arbitrary contrast parameters. Especially in lower temperature, smaller cathode conductivity, larger cathode porosity and lower output voltage, the advantage is more outstanding.

References

1. H. Feng, L. Chen, Z. Xie, F. Sun, *Journal of Power Sources*, 286 (2015) 406.
2. W. Kong, Q. Zhang, X. Gao, J. Zhang, D. Chen, S. Su, *International Journal of Electrochemical Science*, 10 (2015) 5800.
3. M. Ni, *Science Bulletin*, 61 (2016) 1311.
4. W. Kong, Q. Zhang, X. Xu, D. Chen, *Energies*, 8 (2015) 13953.
5. L. Chen, S. Gao, H. Zhang, *International Journal of Electrochemical Science*, 8 (2013) 10772.
6. W. Kong, W. Zhang, S. Zhang, Q. Zhang, S. Su, *International Journal of Hydrogen Energy*, 41 (2016) 16173.
7. T. Li, Z. Wu, K. Li, *Journal of Membrane Science*, 449 (2014) 1.
8. F.P. Nagel, T.J. Schildhauer, S.M. Biollaz, A. Wokaun, *Journal of Power Sources*, 184 (2008) 143.
9. M.F. Serincan, U. Pasaogullari, N.M. Sammes, *Journal of Power Sources*, 192 (2009) 414.
10. M. Krüger, *International Journal of Thermodynamics*, 18 (2015) 95.
11. Y. Shi, C. Li, N. Cai, *Journal of chemical industry and engineering*, 58 (2007) 722.
12. S.-B. Lee, T.-H. Lim, R.-H. Song, D.-R. Shin, S.-K. Dong, *International Journal of Hydrogen Energy*, 33 (2008) 2330.
13. D. Cui, B. Tu, M. Cheng, *Journal of Power Sources*, 297 (2015) 419.
14. L. Zhou, M. Cheng, B. Yi, Y. Dong, Y. Cong, W. Yang, *Electrochimica Acta*, 53 (2008) 5195.
15. J. Jia, S. Shen, S. Riffat, M. Gillott, *Journal of the Energy Institute*, 78 (2013) 76.
16. S. Su, X. Gao, Q. Zhang, W. Kong, D. Chen, *International Journal of Electrochemical Science*, 10 (2015) 2487.
17. W. Kong, J. Li, S. Liu, Z. Lin, *Journal of Power Sources*, 204 (2012) 106.
18. W. Kong, X. Gao, S. Liu, S. Su, D. Chen, *Energies*, 7 (2014) 295.
19. B. Todd, J. Young, *Journal of power Sources*, 110 (2002) 186.
20. H. Zhu, R.J. Kee, *Journal of the Electrochemical Society*, 155 (2008) B715.
21. K.R. Ullah, R.K. Akikur, H.W. Ping, R. Saidur, S.A. Hajimolana, M.A. Hussain, *Energy Conversion and Management*, 94 (2015) 139.
22. M. López-Robledo, M. Laguna-Bercero, J. Silva, V. Orera, A. Larrea, *Ceramics International*, 41 (2015) 7651.
23. N.Q. Duan, D. Yan, B. Chi, J. Pu, L. Jian, *Scientific reports*, 5 (2015)8174.
24. J. Sanyal, G.M. Goldin, H. Zhu, R.J. Kee, *Journal of Power Sources*, 195 (2010) 6671.
25. X. Gao, Q. Zhang, W. Zhang, D. Chen, *International Journal of Electrochemical Science*, 10 (2015) 7521.
26. S. Su, Q. Zhang, X. Gao, V. Periasamy, W. Kong, *International Journal of Hydrogen Energy*, 41 (2016) 16181.